REPORT DOCUMENTATION PAGE

Form Approved
OMB No. 0704-01-0188

PLEASE DO NOT RETURN YOUR FORM TO THE ABOVE ADDRESS.

1. REPORT DATE *(DD-MM-YYYY)*	2. REPORT TYPE	3. DATES COVERED *(From - To)*
10-03-2006	REPRINT	

4. TITLE AND SUBTITLE
Modeling the connection of the global ionospheric electric fields to the solar wind

5a. CONTRACT NUMBER

5b. GRANT NUMBER

5c. PROGRAM ELEMENT NUMBER
61102F

6. AUTHORS
Paul L. Rothwell
John R. Jasperse

5d. PROJECT NUMBER
2311

5e. TASK NUMBER
SD

5f. WORK UNIT NUMBER
A3

7. PERFORMING ORGANIZATION NAME(S) AND ADDRESS(ES)
Air Force Research Laboratory /VSBXP
29 Randolph Road
Hanscom AFB, MA 01731-3010

8. PERFORMING ORGANIZATION REPORT NUMBER
AFRL-VS-HA-TR-2006-1046

9. SPONSORING/MONITORING AGENCY NAME(S) AND ADDRESS(ES)

10. SPONSOR/MONITOR'S ACRONYM(S)
AFRL/VSBX

11. SPONSOR/MONITOR'S REPORT NUMBER(S)

12. DISTRIBUTION/AVAILABILITY STATEMENT
Approved for public release; distribution unlimited.

13. SUPPLEMENTARY NOTES
Reprinted from J. Geophysical Research, Vol. 111, A03211, doi:10.1029/2004JA010992, 2006

14. ABSTRACT
A global ionospheric electrostatic potential model, which we refer to as Nopper-Carovillano (N-C), can be linked with a magnetospheric potential model. The latter model, which we refer to as Hill-Siscoe-Ober (H-S-O), computes a transpolar potential Φ_{PC}(H-S-O) based on solar wind parameters and region-1 field-aligned currents (FAC) from the magnetosheath to the ionosphere. The polar ionospheric conductance required by H-S-O is defined by the N-C model. In this way, the transpolar potential and the associated FAC are the same in both models. A distribution of region-1 FAC in the N-C model predicts a two-cell convection pattern which is in reasonable agreement with plasma drifts measured by Defense Meteorological Satellite Program (DMSP) satellites. The H-S-O model, as modified by N-C, is compared with the Weimer potential model and with the transpolar potentials observed by DMSP satellites during the 6-7 April 2000 magnetic storm. Good agreement is found in both cases. The region-2 (J2) current is estimated from Siscoe (S-RC) ring-current circuit model which is driven by Φ_{PC}(H-S-O). The resistor values in S-RC, as determined by N-C, when combined with the global potential solution, make it possible to estimate the time profile of the equatorial penetration electric field during the storm's main phase. With the values obtained, shielding occurs within 1 hour of onset. Equatorial plasma bubbles (EPBs) are seen some hours after the initial increase of Φ_{PC} and are qualitatively consistent with the equatorial penetration electric field calculated by the combined model.

15. SUBJECT TERMS
Ionospheric electric fields
Solar wind
Transpolar potential

16. SECURITY CLASSIFICATION OF:			17. LIMITATION OF ABSTRACT	18. NUMBER OF PAGES	19a. NAME OF RESPONSIBLE PERSON
a. REPORT	b. ABSTRACT	c. THIS PAGE			Paul L. Rothwell
UNCL	UNCL	UNCL	UNL		19B. TELEPHONE NUMBER *(Include area code)* (781) 377-9664

JOURNAL OF GEOPHYSICAL RESEARCH, VOL. 111, A03211, doi:10.1029/2004JA010992, 2006

Modeling the connection of the global ionospheric electric fields to the solar wind

P. L. Rothwell[1] and J. R. Jasperse[1]

Received 23 December 2004; revised 21 November 2005; accepted 5 December 2005; published 10 March 2006.

[1] A global ionospheric electrostatic potential model, which we refer to as Nopper-Carovillano (N-C), can be linked with a magnetospheric potential model. The latter model, which we refer to as Hill-Siscoe-Ober (H-S-O), computes a transpolar potential Φ_{PC}(H-S-O) based on solar wind parameters and region-1 field-aligned currents (FAC) from the magnetosheath to the ionosphere. The polar ionospheric conductance required by H-S-O is defined by the N-C model. In this way, the transpolar potential and the associated FAC are the same in both models. A distribution of region-1 FAC in the N-C model predicts a two-cell convection pattern which is in reasonable agreement with plasma drifts measured by DMSP (Defense Meteorological Satellite Program) satellites. The H-S-O model, as modified by N-C, is compared with the Weimer potential model and with the transpolar potentials observed by DMSP satellites during the 6–7 April 2000 magnetic storm. Good agreement is found in both cases. The region-2 (J2) current is estimated from the Siscoe (S-RC) ring-current circuit model which is driven by Φ_{PC}(H-S-O). The resistor values in S-RC, as determined by N-C, when combined with the global potential solution, make it possible to estimate the time profile of the equatorial penetration electric field during the storm's main phase. With the values obtained, shielding occurs within 1 hour of onset. Equatorial plasma bubbles (EPBs) are seen some hours after the initial increase of Φ_{PC} and are qualitatively consistent with the equatorial penetration electric field calculated by the combined model.

Citation: Rothwell, P. L., and J. R. Jasperse (2006), Modeling the connection of the global ionospheric electric fields to the solar wind, *J. Geophys. Res.*, *111*, A03211, doi:10.1029/2004JA010992.

1. Introduction

[2] Electrodynamic coupling between the interplanetary medium, the magnetosphere, and ionosphere is subtle and complex. In this paper we will show how this complexity can be approximated by joining three distinct models such that penetration electric fields, which are a possible source for equatorial plasma bubbles, may be estimated from the solar wind. Equatorial plasma bubbles EPBs, for example, have been observed in both ground-based data [*Woodman*, 1970; *Fejer et al.*, 1979; *Fejer et al.*, 1991; *Whalen*, 2001] and satellite measurements [*Fejer et al.*, 1993; *Basu et al.*, 2001; *Huang et al.*, 2002]. Although most equatorial plasma bubbles are generated during quiet periods, *Greenspan et al.* [1991] and *Huang et al.* [2001] noted that major disruptions of the equatorial ionosphere also occur during the early phase of major geomagnetic storms. EPBs are related to the low-latitude ionospheric electric fields which, as pointed out by *Richmond et al.* [2003], have three influences of comparable importance: (1) global winds driven by solar heating, (2) direct penetration of polar cap electric fields to the equator that are partially shielded by the effects of region-2 (J2) field-aligned currents, and (3) disturbance winds driven by high-latitude heating and ion–drag acceleration. In this paper we focus on influence 2, while recognizing the importance of influences 1 and 3.

[3] The penetration of polar cap electric fields to the ionospheric equator has been treated by *Gonzales et al.* [1979], *Spiro et al.* [1988], *Fejer et al.* [1990], *Fejer and Scherliess* [1997], and *Kelley et al.* [2003]. For a recent review, see *Fejer* [2003]. Sophisticated computer simulations by *Spiro et al.* [1988] have carefully treated the time-dependent magnetospheric-ionospheric coupling associated with J2 according to the insights of *Vasyliunas* [1970]. *Senior and Blanc* [1984] developed a self-consistent semi-analytic approach to the same problem. *Scherliess and Fejer* [1997] used the Jicamarca radar observations to study the characteristics and temporal evolution of equatorial dynamo zonal electric fields. As pointed out by *Richmond et al.* [2003], the interplay of the various sources for the equatorial zonal electric field are quite complex with the ionospheric winds, at times, being a major contributor near dusk.

[4] The purpose of the present report is to provide a quantitative method for electrically coupling the interplanetary medium with the equatorial ionosphere. Our method unites three methods that were independently developed. The first method was developed by *Siscoe et al.* [2002] based on the work of *Hill et al.* [1976] and extended by

[1]Space Vehicles Directorate, Air Force Research Laboratory, Hanscom Air Force Base, Bedford, Massachusetts, USA.

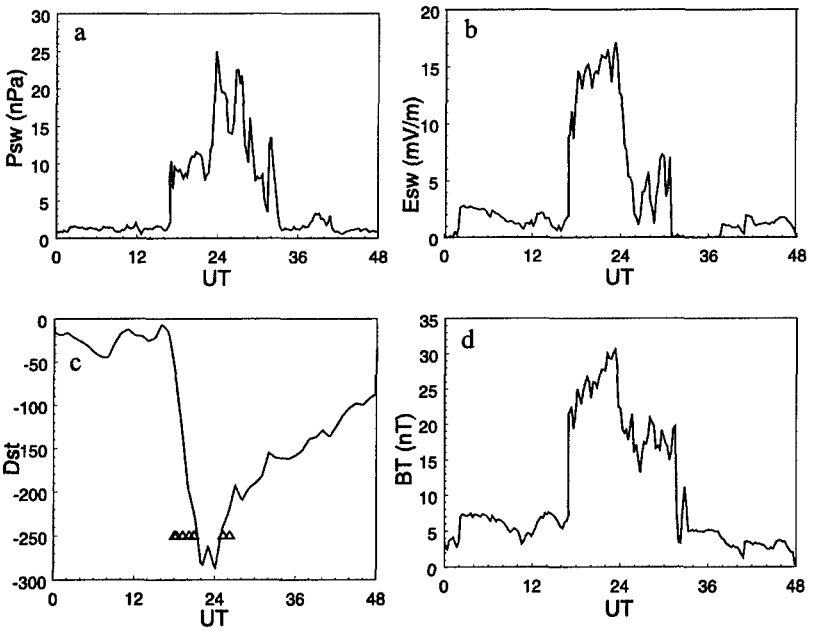

Figure 1. Data for the magnetic storm on 6–7 April 2000. (a) The dynamic pressure of the solar wind plasma at the L1 point. (b) The interplanetary electric field Esw = $|Vx|\ B_T \sin^2(\psi/2)$, where ψ is the "clock" angle between By and Bz. Figure 1d shows the time history of $B_T = \sqrt{(Bx^2 + By^2)}$. (c) Finally, the ring current parameter Dst is shown. Also shown in Figure 1c are the times, denoted by open triangles, at which equatorial plasma depletion bubbles were observed during the magnetic storm. The solar wind variables in Figures 1a, 1b, and 1d were all measured at the L1 point and appropriately shifted in time.

Ober et al. [2003], the Hill-Siscoe-Ober or H-S-O model. In this model, the potential across the polar ionosphere Φ_{PC} and the associated region-1 field-aligned currents (FAC) are determined by solar wind and interplanetary magnetic field parameters. The second approach, developed by *Nopper and Carovillano* [1978] (the N-C model), determines the global ionospheric electric-potential distributions based on the region-1 (J1) and region-2 (J2) currents. The third model is the ring current circuit model (S-RC) developed by *Siscoe* [1982]. In this model Φ_{PC} drives J2 through the ring current, which is presumed to have inductive-like electrical properties consistent with the observation by *Hines* [1963] that gradient drifting ions are gyroenergized by the cross-tail electric field. We join these three models to provide a time-dependent method of estimating the level of electric-field penetration of the solar wind to the equatorial ionosphere.

[5] The penetration of interplanetary electric fields to equatorial latitudes depends on the relative intensity and location of J1 and J2. In short, J1 creates an eastward electric field, while J2 creates a westward (shielding) electric field at equatorial latitudes near the dusk terminator. An eastward electric field tends to enhance the Rayleigh-Taylor instability associated with EPBs (equatorial plasma bubbles) while J2 tends to suppress the instability. It has long been recognized that region-1 currents are closely connected with the trans-polar potential, while region-2 currents arise from the injection of plasma-sheet ions close to the Earth. The effects of high-latitude changes in J1 reach equatorial latitudes at MHD speeds of minutes. On the other hand, the timescale for the buildup of J2 is on the order of hours.

[6] The following sections briefly review the H-S-O and N-C models and then show how we have joined them together with the S-RC model. We have chosen the geomagnetic storm of 6–7 April 2000 to illustrate the combined model. This storm was chosen because, occurring near equinox, it allows us to assume symmetry between the northern and southern ionospheres which therefore removes complications regarding asymmetry. We demonstrate that the results of the combined model are in general agreement with measurements from sensors on spacecraft of the Defense Meteorological Satellite Program (DMSP).

2. Observations

[7] Selected geophysical parameters acquired during the 6–7 April 2000 magnetic storm are shown in Figure 1, with the solar wind parameters shifted in time from the L1 point by the x-component of the solar wind velocity. Figure 1a shows the solar wind pressure Psw, Figure 1b shows the solar wind electric field Esw, and Figure 1d shows the component B_T of the interplanetary magnetic field that is perpendicular to the Earth's magnetic dipole. Dst for the same period is shown in Figure 1c, which also shows the time of bubble occurrence during the storm. The interplanetary electric field is defined by Esw = $|Vx|\ B_T \sin^2(\psi/2)$, where ψ is the "clock" angle between By and Bz [*Sonnerup*, 1974] and Vx is the x-component in GSM coordinates of the solar wind velocity.

[8] Data in Figure 1 show that this storm period was characterized by a sudden, strong, and sustained increase in Esw, Psw, and therefore in Φ_{PC} (Esw, Psw) as discussed

below. The sudden increase in Φ_{PC} required a proportionate increase in the portion of the region-1 FAC directly connected to magnetospheric boundary layers and the magnetosheath. The region-2 system grows in strength over a period of hours due to a delay in plasma response in the inner magnetosphere. Note that the electrical equivalence of inertia is inductance, a feature used in S-RC. The storm followed a single, sustained pulse of energy from the interplanetary medium leading to an immediate and simple main phase to the storm as indicated by the Dst trace.

3. Hill-Siscoe-Ober Model

[9] *Heppner and Maynard* [1987], *Weimer* [1995, 2001, 2005], and others have described the distribution of potential across the high-latitude ionosphere based on measurements, models, theory, or some combination of these. One of the basic components of any of these is the transpolar potential Φ_{PC}, the difference between the maximum potential and minimum polar potential. Numerous studies examined the response of Φ_{PC} to variations of the interplanetary parameters [e.g., *Boyle et al.*, 1997; *Ober et al.*, 2003]. In this paper we use the relationship between Φ_{PC} and the solar wind electric field E_{SW} and dynamic pressure P_{SW} described by *Hill et al.* [1976], *Siscoe et al.* [2002], and *Ober et al.* [2003]. *Hill et al.* [1976] originally suggested that Φ_{PC} may be represented by equation (1).

$$\Phi_{PC} = \frac{\Phi_M \Phi_S}{\Phi_M + \Phi_S} \tag{1}$$

Here Φ_M is the transpolar potential that would result from unhindered dayside merging and Φ_S is the saturation potential obtained when region-1 currents distort the dayside magnetopause to inhibit further merging [*Siscoe et al.*, 2002; *Ober et al.*, 2003]. Φ_{PC} approaches Φ_M during times of low to moderate Esw. Φ_{PC} approaches Φ_S if the Esw becomes very large such as during a major geomagnetic storm. In terms of the solar wind parameters, (1) may be rewritten as shown in (2) using definitions described by *Siscoe et al.* [2002] and *Ober et al.* [2003]. Since we have included the viscous interaction term proposed by *Ober et al.* [2003], we use $\Phi_{PC}(H\text{-}S\text{-}O)$ to denote the transpolar potential (2)

$$\Phi_{PC}(\text{H-S-O}) = \frac{\left[30 P_{sw}^{1/2} + 57.6 E_{sw} P_{sw}^{1/3}\right]}{\left[0.0187\, \xi\, \Sigma_P^P\, P_{sw}^{1/6} + 0.036 E_{sw}\, \xi\, \Sigma_P^P + P_{sw}^{1/2}\right]} \tag{2}$$

[10] The units of Esw and Pw are mV/m and nPa, respectively, and Esw has been previously defined above. In (2), Σ_P^P is the average Pedersen conductance over the polar cap. *Ober et al.* [2003] used the solar radio flux at 10.7 cm (F10.7) as a proxy for the extreme ultraviolet (EUV) radiance to estimate Σ_P^P as given by *Robinson and Vondrak* [1984]. In the present work we use the Robinson-Vondrak formula, $\Sigma_P^P = 0.88\,(\text{F10.7} \cos\chi)^{1/2}$, with the solar zenith angle χ equal to 80° to represent the average polar cap conductance as shown in (3).

$$\Sigma_P^P = 0.37\sqrt{\text{F10.7}} \tag{3}$$

[11] Given a set of values for E_{sw}, Psw, and F10.7, one can use (2) and (3) to estimate the magnitude of Φ_{PC}(H-S-O). Note the sensitivity of Φ_{PC}(H-S-O) to the polar cap conductance, particularly when Σ_P^P is on the order of a few Siemens. *Siscoe et al.* [2002] use Ohm's law to obtain the total region-1 current (J1) into and out of the high-latitude ionosphere in response to the applied potential drop $\Phi_{PC}(H\text{-}S\text{-}O)$. For consistency arguments regarding (2) and (4), refer to *Siscoe et al.* [2002, 2004]

$$J1 = \xi\, \Sigma_P^P\, \Phi_{PC}(\text{H-S-O})$$

$$\xi = 4.45 - 1.08 \log \Sigma_P^P \tag{4}$$

[12] With *Siscoe et al.* [2002] we assume (4) is the total J1 even though J1 may be partially observed on closed field lines. The parameter ξ scales the Pedersen current closure across the polar cap to a "single-wire" approximation. *Siscoe et al.* [2002] did not try to describe the distribution of current into and out of the region 1 system or to describe the resulting distribution of ionospheric potentials.

4. Nopper-Carovillano Model

[13] The N-C model solves the current continuity equation to determine the global distributions of electric potential. A specification of the distributions of J1 and J2 FAC and global ionospheric conductance is required. Transpolar potentials, which are labeled by $\Phi_{PC}(N\text{-}C)$ in this model, are determined from maxima and minima of the calculated polar potential distributions (see Figure 2). Once the global ionospheric conductance is defined, then the N-C model determines the effective polar cap conductance $\xi\Sigma_P^P$ by finding $\Phi_{PC}(N\text{-}C)^{-1}$ for J1 = 1 MA, J2 = 0, keeping in mind that Φ_{PC} is in kilovolts. Consistency requires that this value for $\xi\Sigma_P^P$ be used in (2) for determining Φ_{PC}(H-S-O). If the J1 input to the N-C model is set equal to that of (4), then $\Phi_{PC}(N\text{-}C) = \Phi_{PC}$(H-S-O). The joint model is now able to describe the penetration of interplanetary electric fields to both the polar and low-latitude ionosphere.

[14] The N-C model provides a flexible method for the distribution of the total field-aligned current (FAC) flowing into and out of region 1 (J1) and region 2 (J2). The specified J1 and J2 currents enter and exit the ionosphere but are constrained to close in a two-dimensional conducting shell. *Siscoe and Maynard* [1991] developed a similar method for distributing FACs and deriving ionospheric potential distributions.

[15] The N-C approach uses a system of spherical coordinates whose origin is at the center of the Earth. The z-axis passes through the magnetic north pole. Initially, a three-dimensional expression for **J** is reduced to two dimensions by imposing the condition Jr = 0. Under this constraint the two-dimensional shell current **J** and conductance tensor Σij are given by

$$J_\theta = \Sigma_{\theta\theta} E_\theta + \Sigma_{\theta\varphi} E_\varphi \qquad J_\varphi = -\Sigma_{\theta\varphi} E_\vartheta + \Sigma_{\varphi\varphi} E_\varphi \tag{5}$$

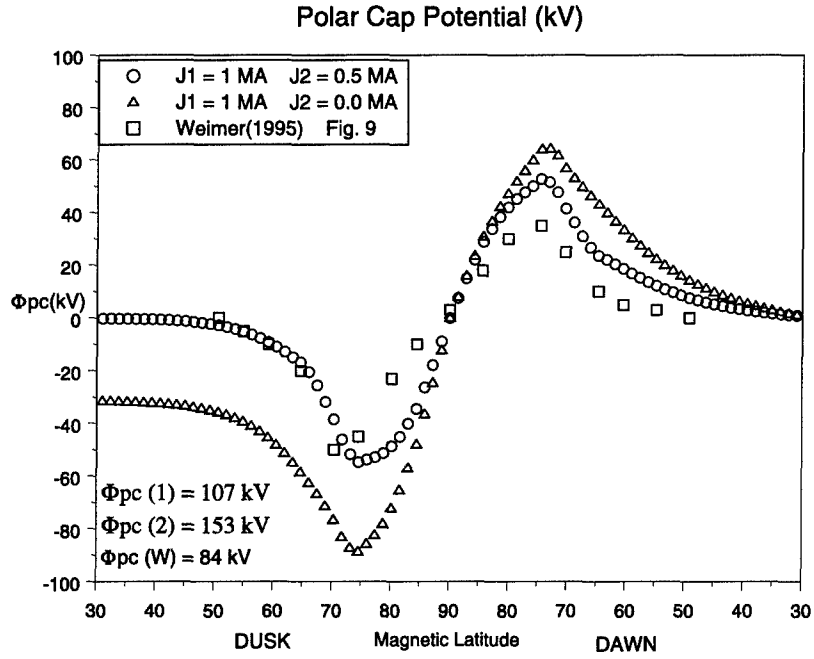

Figure 2. A comparison of the Nopper-Carovillano model with that of *Weimer* [1995]. The conditions are for equinox using the default N-C conductance model (16). The N-C results for the polar potential are for J1 = 1.0 MA. The open circles show the solution in the dusk-dawn meridian for J2 equal 0.5 MA. The open triangles are for zero J2. Note that the effect of adding J2 is to lower the polar cap potentials. We have included, using the open squares, the potentials from Figure 9 of *Weimer* [1995] for comparison. The transpolar potential Φ_{PC}*(N-C)* is defined to be the be the difference between the maximum and minimum voltages and, as shown in the text, can be identified with the transpolar potential of Hill-Siscoe-Ober.

where E_θ and E_φ represent the colatitude and azimuthal components of the electric field, respectively. The conductance related terms are defined as

$$\Sigma_{\theta\theta} = \frac{\Sigma_0\Sigma_p}{D} \qquad \Sigma_{\varphi\theta} = \frac{\Sigma_0\Sigma_H \sin(I)}{D}$$
$$\Sigma_{\varphi\varphi} = \frac{\Sigma_0\Sigma_p \sin^2(I) + \left(\Sigma_p^2 + \Sigma_H^2\right)\cos^2(I)}{D} \qquad (6)$$
$$D = \Sigma_0 \sin^2(I) + \Sigma_p \cos^2(I)$$

where Σ_p represents the Pedersen and $\Sigma_H = 2\Sigma_p$ represents the Hall conductance. Σ_o denotes the conductance parallel to **B**, which *Nopper* [1978] takes be 31.6 times Σ_p. The symbol I denotes the dip angle of the Earth's magnetic dipole field. We presently assume that the dipole axis is aligned with the Earth's spin axis and perpendicular to the Earth-Sun line. Otherwise, the dip angle is a function of geographic longitude, which significantly increases the complexity of (6). Therefore as the model now stands, longitudinal effects are not included. With the substitution $\mathbf{E} = -\nabla\Phi$ the current continuity equation reduces to a Poisson-type equation [*Vasyliunas*, 1970]

$$\nabla \cdot [\Sigma \cdot \nabla\Phi] = j_{\parallel} \sin(I), \qquad (7)$$

where $j_{\parallel}$ is the specified distribution of FAC associated with J1 and J2. Note that $j_{\parallel}$ is equivalent to a positive charge density for downward current and a negative charge density for upward current.

[16] Equation (7) is solved by numerical computation using the multigrid method [*Press et al.*, 1992; *Briggs et al.*, 2000; *Trottenberg et al.*, 2001], a method that capitalizes on the fact that the Fourier components of the potential converge at different rates. A 129 × 129 (16,641 points) global grid was used to solve for the distribution of ionospheric potentials. Following the example given by *Nopper and Carovillano* [1978, 1979], the J1 and J2 currents are distributed in two crescent regions extending 120° in magnetic local time at 72° and 66° magnetic latitude, respectively. Each crescent region is centered on the dusk-dawn meridian. Each current region is 3° wide. For our computations, the current region dimensions are 32 by 2 grid spacings. The total current for each current region is uniformly distributed throughout the region. In this way a baseline model may be constructed for comparison with data.

[17] *Nopper and Carovillano* [1978] used a globally varying conductance pattern which varied from a solar-zenith angle of −90° to +90° with enhancements at the auroral oval. However, in assuming symmetry between the northern and southern hemispheres, they implicitly solved (7) only for equinox cases. In order to use their formulation with as little modification as possible, a geomagnetic storm near the equinox was chosen to illustrate our computations.

[18] Figure 2 provides two examples of N-C model solutions for potential distributions along the dusk-dawn

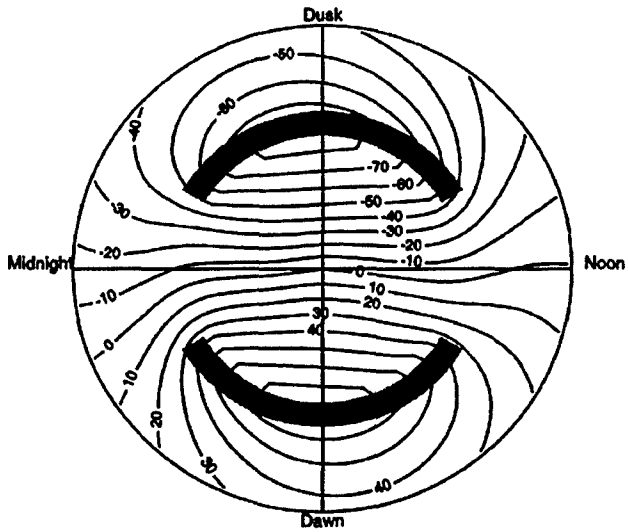

Figure 3. Electric potentials from 60° magnetic latitude to the north pole with the J1 current shown as a pair of gray crescents. The magnitude of J1 is determined by the Hill-Siscoe-Ober model and conditions in the interplanetary medium. In this case, there is no region-2 current system. Contour values are in kilovolts.

meridian. These plots were obtained using the ionospheric conductance as given in (16) below. With region-1 and region-2 current distributions described above, we set J1 = 1.0 MA and J2 = 0.5 MA (open circles) or 0.0 MA (open triangles). The plots in Figure 2 show that with J2 = 0.5 MA, $\Phi_{PC}(N\text{-}C)$ = 107 kV, and with J2 = 0 MA, $\Phi_{PC}(N\text{-}C)$ = 153 kV. In the present configuration, we are simply looking at the response of a two-dimensional conductive ionosphere to freely chosen J1 and J2 FAC. In section 5 a transpolar potential and a ring current is added to the model.

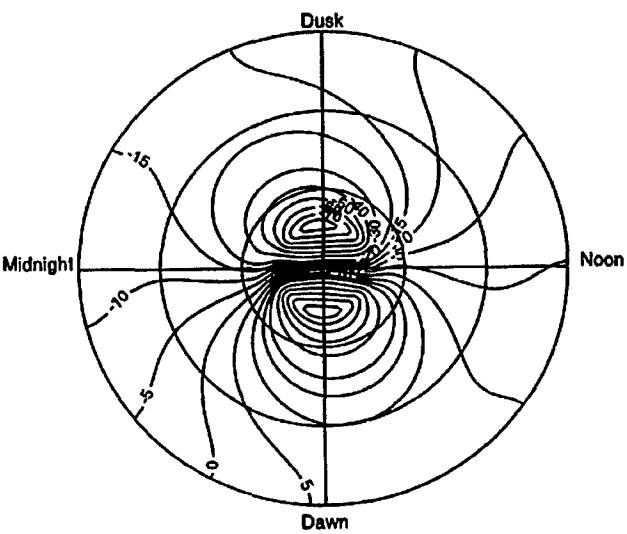

Figure 4. The electric potential from the magnetic equator to the north magnetic pole computed from the Nopper-Carovillano model for the condition described in the Figure 3. This highlights the direct penetration of the polar electric fields to equatorial latitudes.

[19] A typical ionospheric N-C polar potential pattern is given in Figure 3 together with a pair of shaded regions showing where the J1 current enters and leaves the ionosphere. The equipotential lines bend as they cross the polar region from the noon to midnight sectors due to the gradient in the conductance. The model has not been adapted to show the influence of IMF B_y [*Weimer*, 1995] which was relatively small between 1700 and 2400 UT on 6 April 2000.

[20] For weak J2 the electric potentials extend equatorward of the auroral boundary ($\lambda_m \sim 63°$). Figure 4 shows that the ionospheric potential driven by the interplanetary medium extends to the magnetic equator. Because the conductance in the two poles is assumed to be the same, contributions from the two hemispheres are nearly the same and the N-C electric field at the equator has only an azimuthal component. With *Nopper and Carovillano* [1978], we note that *Wolf* [1970] demonstrated the necessity of an eastward electric field component in the early evening sector to maintain current continuity across the conductance gradient at the dusk meridian. In Appendix A, we illustrate some ionospheric features obtainable with N-C.

5. Siscoe Ring Current Model

[21] Since one goal is to determine the time-dependent penetration electric fields at lower latitudes, we need a model for J2. For present purposes we use that of *Siscoe* [1982] (S-RC), as seen in Figure 5. Here Φ_{PC} drives a current J1 that splits into a transpolar component and J2′ that partially closes across Rs at lower latitudes and partially across an inductor-equivalent L in the magnetosphere, which represents the ring current. To get a better handle

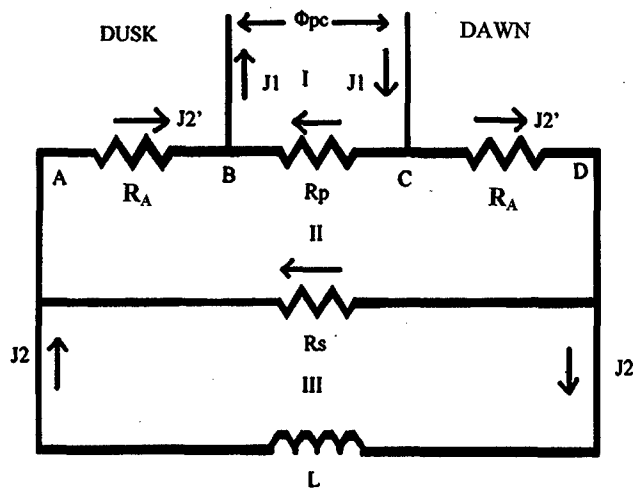

Figure 5. Taken from *Siscoe* [1982]. Rp is the average resistance across the polar cap. B and C locate the upward and downward legs of J1, respectively. J2 enters the ionosphere at point A and exits the ionosphere at D. The ionospheric resistance between A and B and C and D is R_A. Rs represents the effective resistance of the ionosphere at lower latitudes to closing current J2′−J2. Therefore in this model J1 also provides sufficient current to close at lower latitudes, across the poles, and J2 into the magnetosphere.

on L, let us visualize a fraction of Φ_{PC} being applied across closed field lines in the magnetotail corresponding to points A and D in Figure 5. As is well-known, this results in an earthward $\mathbf{E} \times \mathbf{B}$ drift with the ions gradient-curvature drifting westward. *Hines* [1963] showed that gradient drift causes perpendicular heating of westward drifting ions at a rate $q\mathbf{V_d} \cdot \mathbf{E}$, where q is the ion electrical charge and $\mathbf{V_d}$ the ion drift velocity due to the magnetic field gradient. The ring current therefore has inductor-like properties, storing energy in the ion gyromotion instead of the magnetic field. The parameter L in the S-RC model (Figure 5) reflects this property. The *Siscoe* [1982] model is intended to describe the main phase of a magnetic storm.

[22] In Figure 5, Kirchhoff's law is satisfied in each of the three loops, I, II, and III, as now shown.

$$\text{I.} \quad (J1 - J2')Rp = \Phi_{PC}, \quad J1 = \Phi_{PC}/Rp + J2' \tag{8}$$

$$\text{II.} \quad (J2' - J2)Rs + 2R_A J2' = \Phi_{PC} \tag{9}$$

$$\text{III.} \quad LdJ2/dt + (J2 - J2')Rs = 0 \tag{10}$$

Solve (9) for J2′, find J2 − J2′, and then substitute into (10).

$$LdJ2/dt + 2R_A RsJ2/(Rs + 2R_A) = Rs\ \Phi_{PC}/(Rs + 2R_A) \tag{11}$$

Equation (11) is easily solved.

$$J2 = \Phi_{PC}/(2R_A)(1 - \exp(-t/\tau)) \tag{12}$$

$$\tau = L(Rs + 2R_A)/(2R_A Rs) \tag{13}$$

for a step like ϕ_{PC}. J2′ is found as

$$J2' = \Phi_{PC}/(Rs + 2R_A)[1 + Rs/(2R_A)(1 - \exp(-t/\tau))]. \tag{14}$$

Therefore from (8)

$$J1 = \Phi_{PC}[1/Rp + 1/(Rs + 2R_A) + Rs/(2R_A(Rs + 2R_A)) \cdot (1 - \exp(-t/\tau))] \tag{15}$$

[23] The first term on the right-hand side of (15) denotes the part of J1 crossing the polar cap, and the next two terms represent the part of J1 flowing toward lower latitudes including J2 (i.e., the fraction of J2' that is diverted to the magnetosphere). In the limit of large t, $J1 = \Phi_{PC}/Rp + J2$. The transpolar potential drives whatever currents are required (region-1) into the dawn ionosphere and out of the dusk ionosphere. Part of this current directly crosses the polar cap and the rest flows equatorward, splitting into region-2 current and current that flows through the low-latitude and midlatitude ionosphere. If the region-2 current system is fully developed, it tends to shield (cancel) the region-1 electric field and currents, especially at lower latitudes. This model is consistent with satellite magnetometer measurements [*Zmuda and Armstrong*, 1974a, 1974b; *Iijima and Potemra*, 1976; *Smiddy et al.*, 1980] that see region-1 and region-2 currents as adjacent pairs, a downward J1 and an upward J2 on the dawnside, and an upward J1, downward J2 on the duskside.

Table 1. Transpolar Potentials and Equatorial Electric Fields From the N-C Model, $\alpha = 0$, $\beta = 3.8$[a]

Σ_P^P, S	Σ_A, S	ξ	$\xi\Sigma_{P_1}^P$, S	$\Phi_{PC\ 1}$, kV	Eeq1, mV/m	Eeq2, mV/m
		J1 = 1 MA		*J2 = 0*		
4.8	0	2.01	9.8	101.3	1.2	−2.7
5.6	3	2.44	13.7	72.9	1.0	−1.9
5.9	4	2.51	15.0	71.9	0.8	−1.6
7.0	8	2.86	20.0	50.0	0.4	−0.8
9.1	16	3.43	31.2	32.0	0.2	−0.5

[a]With the average polar cap Pedersen conductance Σ_P^P defined as a function of the auroral conductance Σ_A, the transpolar potential Φ_{PC} and the corresponding equatorial electric fields Eeq1 and Eeq2 are found for J1 and J2. Eeq1 and Eeq2 are taken as the best estimates of the pre-reversal maximum and minimum, respectively. Eeq2 is found with J1 = 0, J2 = 1 MA.

6. Combined Model

[24] Using N-C, it is possible to reduce the distributed polar current-voltage relation to a "single-wire" with an effective conductance $\xi\Sigma_P^P$, between the maxima and minima voltages as shown in Figure 2 and as described above. This allows us to combine the N-C and H-S-O models as the corresponding voltages are applied across the same "wire." The N-C model is used to determine $\xi\Sigma_P^P$, as stated, by finding the ratio $J1/\Phi_{PC}$*(N-C)*, usually with J1 = 1 MA and J2 = 0 MA. The parameter ξ partially depends on the geometry of the inputted currents and partially on the ionosphere presenting an impedance equivalence of two parallel resistors. The average Pedersen conductance Σ_P^P can be independently found by a Monte Carlo averaging of the model conductance (17) over the polar cap. By using this approach we find $\xi = 2.0$–3.4 (see Table 1). Again, consistency requires that the same value of $\xi\Sigma_P^P$ be used in determining Φ_{PC}(H-S-O) from (2).

[25] The ionospheric conductance model can be made more realistic by incorporating its global dependence on the EUV flux (via the proxy of the F10.7 solar radio flux). The global Pedersen conductance $\Sigma p(\theta, \varphi)$ as given by *Nopper and Carovillano* [1978] is shown in (16).

$$\Sigma p(\theta,\varphi) = 0.3 + 5.0\exp\left\{-\left[\cos^{-1}(\sin(\theta)\cos(\varphi))\right]^2/1.804\right\} + \text{auroral terms} \tag{16}$$

auroral terms = $\Sigma_A \exp(-(\theta - \theta_A)^2/\sigma_A^2)$; $\Sigma_A = 3$ S, $\sigma_A = 0.57°$, $\theta_A = 20°$. This expression can be extended to arbitrary F10.7 values by using the parameters α and β.

$$\Sigma p(\theta,\varphi) = \Sigma_P^P\left(\alpha + \beta\exp\left\{-\left[\cos^{-1}(\sin(\theta)\cos(\varphi))\right]^2/1.804\right\}\right) + \text{auroral terms} \tag{17}$$

The average polar conductance Σ_P^P due to solar EUV (F10.7) is defined in (3). This implies that for the 6–7 April 2000 time period when F10.7 = 177, $\Sigma_P^P = 4.9$ S. We now adjust α and β, as given in (17), to obtain an appropriate conductance value at the subsolar point. For example, if $\alpha = 0$ and $\beta = 3.8$, one obtains a subsolar conductance of 19 S

[*Senior and Blanc*, 1984]. The α parameter is set to zero to emphasize the local time dependence of (17). Consistency requires $\Sigma_P^P = \langle \Sigma p(\theta, \varphi) \rangle$, where the brackets denote averaging over the polar cap. We find that $\langle \Sigma p(\theta, \varphi) \rangle$ = 4.8 S in comparison with the value of 4.9 S obtained from (3). It is concluded that with these values for α and β, (17) is a reasonable representation of the global ionospheric conductance on 6–7 April 2000. Having defined the global ionospheric conductance we can directly relate the ionospheric electric fields at any location in the ionosphere to E_{SW}. In Appendix A we show some of the high- and low-latitude features of N-C.

7. Application of the Combined Model

[26] In the present approach there are three models that form a basic solar wind-magnetosphere-ionosphere model. According to the Hill-Siscoe (H-S) model, the solar wind at L1 determines the transpolar potential Φ_{PC} over the polar caps, consistent with the polar conductance predicted by the ionospheric model (N-C). The results are shown to be in good agreement with both the empirical *Weimer* [2005] transpolar potentials and DMSP measurements for the 6–7 April 2000 magnetic storm. The region-1 and region-2 (J2) currents are estimated from the Siscoe (S-RC) ring-current circuit model which is driven by Φ_{PC}. The resistor values in S-RC are determined by N-C which, when combined with the global potential solution, make it possible to estimate the time profile of the equatorial penetration electric field during the storm's main phase. Applying this approach to the 6–7 April 2000 storm, we find that shielding occurs within 1 hour of onset.

[27] The J2 rise time is estimated using the Dessler-Parker-Scopke (DPS) [*Dessler and Parker*, 1959; *Scopke*, 1966] relation. In this manner, expressions for J1 and J2 are found that, when combined with the equatorial electric fields estimated from N-C, give a time-dependent expression for shielding. It is to be noted that the obtained shielding times tend to be much shorter than the J2 rise times.

7.1. High Latitudes

[28] A key feature therefore is to accurately define the polar ionospheric conductance during the 6–7 April 2000 magnetic storm. We do this by considering five values of auroral conductance, Σ_A = 0, 3, 4, 8, and 16 S, in determining $\xi\Sigma_P^P$. The five corresponding values of $\xi\Sigma_P^P$, when put into (2), give five curves for Φ_{PC}(H-S-O) (see Figure 6c) throughout the 6–7 April 2000 magnetic storm. These curves are then compared with the experimental Φ_{PC}(DMSP) values for the transpolar potential as shown in Figure 6B. We then choose the value of Σ_A for which Φ_{PC}(H-S-O) and Φ_{PC}(DMSP) are the best match. In this case Σ_A = 3 S. This value of Σ_A is also consistent with the observed electron precipitation energy using the formula of *Robinson et al.* [1987]. The "standard" value for $\xi\Sigma_P^P$ during the 6–7 April 2000 storm is therefore 13.7 S as given in Table 1.

[29] By using N-C to define the conductance $\xi\Sigma_P^P$ for the H-S-O model (2), we find good agreement with the *Weimer* [2005] empirical potential model for this magnetic storm, as shown in Figure 6a. Note that the Weimer model is based on DE-2 satellite data taken between August 1981 and March 1983. During this period the value of F10.7 was 178 ± 33 compared with 177 for the present magnetic storm which indicates the comparison is being made under similar conditions of global EUV conductance. In the *Weimer* [2005] model a parameterized exponential function is used to model saturation effects in contrast to the H-S-O expression given in (2). Note that the agreement between the Weimer and H-S-O models is dependent on $\xi\Sigma_P^P$, as calculated by N-C. Therefore Figure 6a represents an overall consistency between these three models.

[30] Experimental values of the transpolar potentials shown in Figure 6b were derived from data taken on board DMSP satellite F13. During the 6–7 April 2000 magnetic storm satellite F13 approached the center of the N-C potential cells shown in Figure 3, particularly during northern passes. Under these conditions good agreement was found between the measured potentials and the values predicted by N-C. Therefore Φ_{PC}(DMSP) was estimated from the potential minima and maxima [*Rich and Hairston*, 1994] and plotted as open squares in Figure 6b. Note that the DMSP results generally agree with those of Weimer in Figure 6a.

[31] Figure 6c shows five time histories of Φ_{PC}(H-S-O) as determined by the ACE satellite solar wind measurements. The five curves represent the five values of auroral conductance Σ_A as given in Table 1 with the solar wind parameters shifted to later times consistent with the solar wind velocity. The five curves in Figure 6c represent the effect of enhanced auroral conductance on Φ_{PC}(H-S-O). In other words, auroral precipitation suppresses Φ_{PC}(H-S-O). Roughly, there is about a 16 kV decrease in Φ_{PC}(H-S-O) for each 1 S increase in Σ_A between 0 and 3 S.

7.2. Equatorial Regions

[32] Now let us derive the equatorial electric field Eeq using the N-C model. The N-C model is treated as a numerical Green's function. That is, for a fixed geometry and global conductance the potential and electric fields at specific locations are determined by independently inputting 1 MA values for J1 and J2. The corresponding potential and electric field values at these locations for arbitrary J1 and J2 may then be found by scaling and superposition. We denote Eeq1 for the prereversal enhancement electric field from J1 and Eeq2 as the corresponding minimum (negative) electric field from J2.

[33] Table 1 lists the results for $\Phi_{PC}(N\text{-}C)$ and the equatorial electric fields Eeq1 and Eeq2 using the five values of the auroral conductance Σ_A, 0,3, 4, 8, and 16 S [*Gonzales et al.*, 1983]. For each case a J1 = 1 MA current is put into the N-C model as being evenly distributed into and out of two 120° crescents at λm = 72° centered at the dusk and dawn meridians. Consistent with the standard convention J1 enters the ionosphere on the morningside and exits on the duskside. The crescents have a width of 3° so that a 1 MA current corresponds to a parallel current density of 0.72 $\mu A/m^2$. The region 2 current J2 is placed at 66°, just equatorward of J1, also with a width of 3° and extending 120° in longitude. J2, of course, has the opposite sense of entering and exiting the ionosphere as does J1. In the present instance J2 = 1 MA corresponds to a parallel current density of 0.56 $\mu A/m^2$.

[34] It should be pointed out that although for modeling purposes we keep the latitudes of J1 and J2 fixed throughout

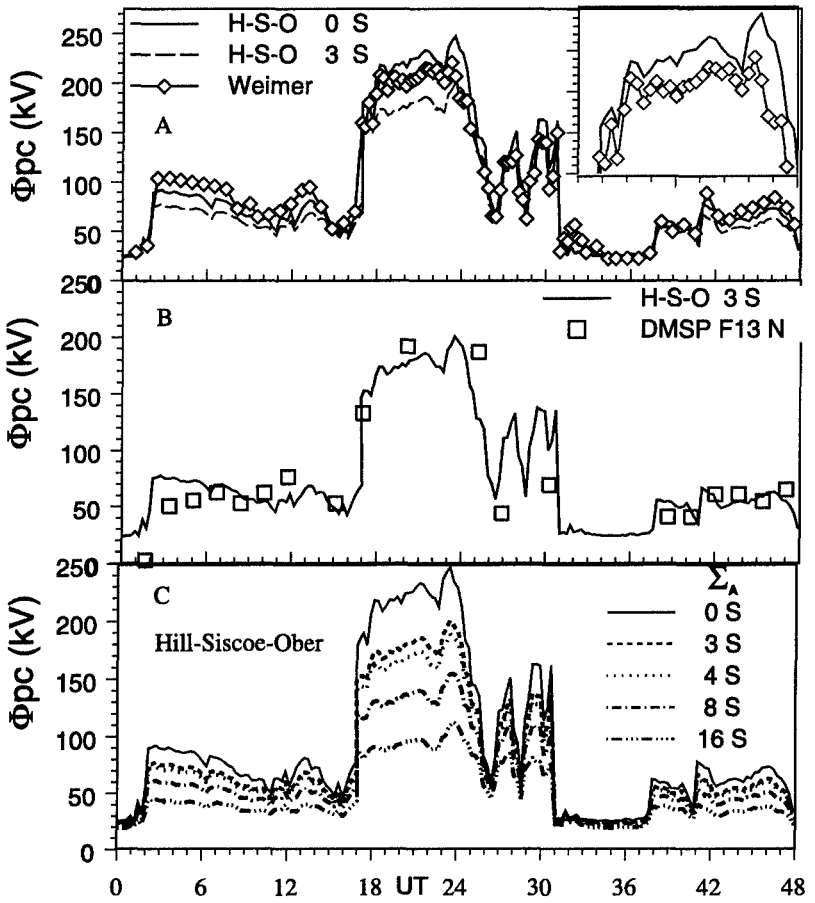

Figure 6. (a) Comparison of the transpolar potential Φ_{PC} from the *Weimer* [2005] model for the 6–7 April 2000 magnetic storm with that from the H-S-O model for zero and three Siemens auroral conductance. The inserted plot ranges from 1600 UT on 6 April to 0100 UT on 7 April (in one hour intervals) in order to highlight peak details. The y-axis ranges from 150 to 250 kV in 25 kV steps. (b) The Σ_A = 3 S H-S-O curve is compared with corrected DMSP measurements of the transpolar potential during the same storm using the N-C model. We use only northern passes of satellite F13 as these go more directly through the potential cell centers. (c) The H-S-O transpolar potential as calculated at various levels of auroral conductance as shown. Note the sensitivity of the results at lower values of Σ_A. On the basis of the electron precipitation energy, Σ_A = 3 S is considered to be the correct theoretical curve.

the storm, it is recognized that during the course of the storm the auroral zone moved to lower latitudes. The auroral oval boundaries expand equatorward after significant net open flux has been added to the polar cap [*Siscoe and Huang*, 1985] and the plasma sheet convects close to Earth [*Crooker and Siscoe*, 1983]. This expansion occurred with a lag of about 3 hours between the beginning of the storm and the time of significant equatorward movement [*Huang and Burke*, 2004].

[35] From Table 1 and Figure 6c it is also seen that a higher auroral conductance depresses Φ_{PC} $\Phi_{PC}(N\text{-}C)$ at constant J1. Put another way, the polar ionosphere with a higher conductance demands a larger current in order to sustain the same value of Φ_{PC}. This causes saturation of Φ_{PC} to occur at lower values as can be seen from (2).

[36] We now turn to the penetration electric field as calculated by N-C. The conductance gradients arising from (17) cause J1 to create a "prereversal" enhancement in Eeq on the eveningside, although significantly displaced from its proper location at 1800 MLT [*Fejer*, 1997]. It is found that this displacement is due to the approximate nature of (17), which does not contain the small-scale features of the terminator conductance. The equatorial electric fields are essentially fringe electric fields and therefore are sensitive to source location. They are also difficult to calculate accurately because of strong conductance gradients near the equator from dip angle effects and density gradients. However, one modification including density gradient effects near the terminator was used with the results shown in Figure 7 for Eeq1. There is a similar curve for Eeq2, but with the opposite sign and larger amplitude. For modeling purposes we use the extremum (prereversal) values of Eeq1 and Eeq2 as found from N-C with J1 and J2 separately set equal to 1 MA, as shown in Table 1. One sees from Table 1 that Eeq2 ~ -2 Eeq1, which reflects sensitivity to the location of the source currents, since J2 is closer to the equator. It is well known that during a magnetic storm both J1 and J2 move closer to the

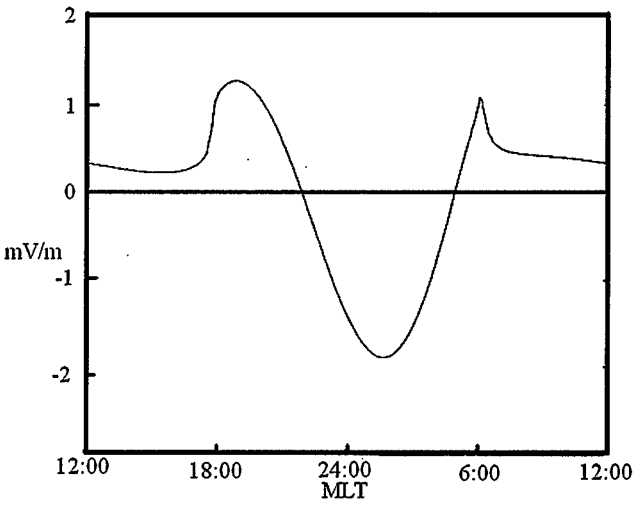

Figure 7. The equatorial electric field Eeq1 as a function of MLT, J1 = 1 MA, $\lambda m = 72°$, and J2 = 0 MA. This calculation included an additional density gradient at the terminator which placed the pre-reversal enhancement near 1800 MLT. The calculation was performed using a banded-matrix method as described by *Press et al.* [1992]. A similar curve is found for Eeq2 (J1 = 0 MA, J2 = 1 MA, $\lambda m = 66°$), but of the opposite sign and with a larger amplitude. Note that the integral of Eeq around the equator is zero, since curl E = 0.

equator. However, it is found that, at present, because the net Eeq is a small difference of two relatively large numbers the error in the penetration electric field Eeq becomes too large if J1 and J2 move substantially equatorward. This feature will be addressed in future work.

[37] A decrease in magnitude of both Eeq1 and Eeq2 occurs as the auroral conductance Σ_A increases (Table 1). On the other hand, both Eeq1 and Eq2 are linearly related to J1 and J2, respectively, as expected from Poisson's equation. Therefore one can apply superposition in finding the net Eeq for fixed Σ_A. Note also, however, that the equatorial ionosphere is three-dimensional, not two-dimensional as treated here. This feature may make a significant change in the present values of Eeq.

[38] By using the results from Table 1 and superposition we have the following relation for each specified value of Σ_A.

$$\text{Eeq(mV/m)} = \text{Eeq1 J1(MA)} + \text{Eeq2 J2(MA)} \qquad (18)$$

Equation (18) gives a simple representation of the "prereversal" electric field as a function J1 and J2. However, as shown above, S-RC indicates that J1 and J2 are coupled, so we have the more complex expression (19) for the penetration electric field Eeq(t) from inputting (12) and (15) into (18).

$$\begin{aligned}\text{Eeq}(t) = {} & \Phi_{PC}(1/\text{Rp} + 1/(\text{Rs} + 2R_A) + \text{Rs}/(2R_A(\text{Rs} + 2R_A)) \\ & \cdot (1 - \exp(-t/\tau)))\text{Eeq1} + \Phi_{PC}/(2R_A) \\ & \cdot (1 - \exp(-t/\tau))\text{Eeq2} \end{aligned} \qquad (19)$$

7.3. Using N-C to Define the Resistors in S-RC

[39] Owing to the tensor nature of the ionospheric conductance (6) finding values for the resistors shown in Figure 5 is not obvious. However, since only the diagonal components of the conductance tensor contribute to energy dissipation ($\mathbf{J}\cdot\mathbf{E} \neq 0$), the reciprocals of $\langle\Sigma_{\theta\theta}\rangle$ and $\langle\Sigma_{\varphi\varphi}\rangle$ can be used to determine Rp, R_A, and Rs, where the bracket denotes an average value. From Figure 5 it is immediately seen that an applied voltage across BC, which represents the polar cap, is equivalent to placing a voltage across two resistors in parallel, with L removed from the circuit. For two resistors in parallel the total conductance is the sum of the two individual conductances. This is partially why the ξ parameter, in the present treatment, varies between 2 and 3.4 in Table 1.

[40] The centers of the polar potential cells coincide with the location of the region-1 (J1) currents. Therefore points B and C in S-RC (Figure 5), in the present treatment, correspond to 72° magnetic latitude in the N-C model. In a similar manner, points A and D (J2) in Figure 5 correspond to 66° in magnetic latitude. The cross-cap Pedersen current flows mainly in the θ direction so that, using (17) and (6) for magnetic latitudes between 72° and 90°, $\text{Rp} = \langle\Sigma_{\theta\theta}\rangle^{-1} = 0.174\ \Omega$. Throughout, Σ_A is set equal to 3 S.

[41] We now want to estimate $2R_A$ in Figure 5. The average conductance $\langle\Sigma_{\theta\theta}\rangle$ between 66° and 90° in magnetic latitude (points A and D) is found such that $\text{Rp} + 2R_A = \langle\Sigma_{\theta\theta}\rangle^{-1} = 0.210\ \Omega$. A value of 0.174 Ω has just been found for Rp so that $2R_A = 0.036\ \Omega$.

[42] To determine Rs, we consider a circuit-equivalent equatorward of 66°. The low-latitude currents close by flowing equatorward from 66° in latitude on the dawnside and then azimuthally in two paths, pass noon and midnight, where they flow poleward to close on the duskside. The S-RC resistor Rs therefore is composed of two parallel azimuthal resistors, one for the dayside and one for the nightside, and two meridian resistors representing dusk and dawn. We find from the N-C model $\langle\Sigma_{\theta\theta}\rangle$ (dawn) = 30.65 S, $\langle\Sigma_{\theta\theta}\rangle$ (dusk) = 30.22 S, $\langle\Sigma_{\varphi\varphi}\rangle$ (day) = 16.56 S, $\langle\Sigma_{\varphi\varphi}\rangle$ (night) = 2.75 S. As expected, most of the current closes on the dayside. The value for the resistor Rs is now given in (20).

$$\text{Rs} = 1/30.65 + 1/30.22 + 1/(16.56 + 2.75) = 0.117\,\Omega \qquad (20)$$

In summary, the following values for the three resistors are Rp = 0.174 Ω, $2R_A$ = 0.036 Ω, and Rs = 0.117 Ω.

7.4. Using DPS to Estimate J2 Rise Time

[43] The rise time for J2 may be estimated from the Dessler-Parker-Scopke (DPS) [*Dessler and Parker*, 1959; *Scopke*, 1966] relation that relates Dst with the total ring current energy. Including Earth conductivity effects, a 100 nT decrease in Dst corresponds to 2.8×10^{15} J of ring current energy [*Kivelson and Russell*, 1997]. In terms of the present model this relation can be recast as

$$^1/_2 L\ J2^2 = 2.8 \times 10^{13}|\text{Dst}|. \qquad (21)$$

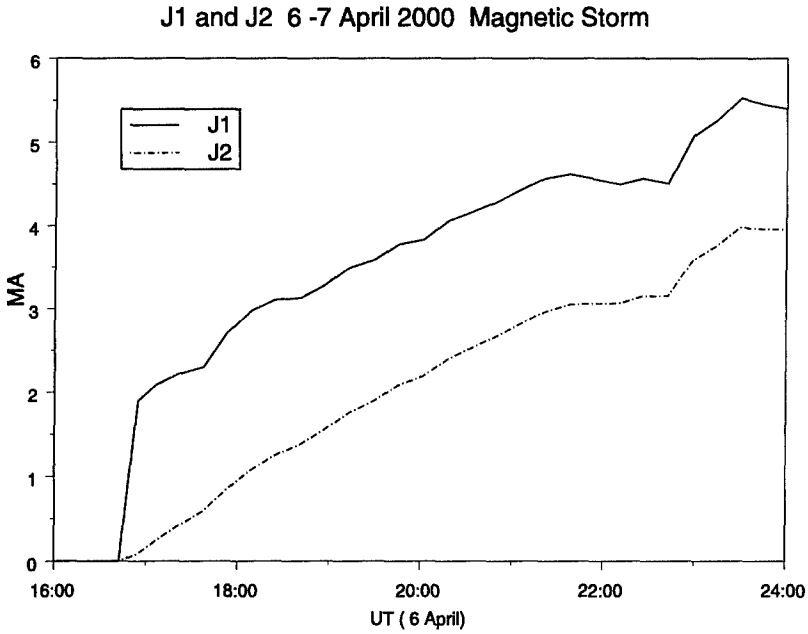

Figure 8. Model time history of J1 and J2 currents during the 6–7 April, 2000 magnetic storm using (15) and (12), respectively, based on the model described by *Siscoe* [1982] and as shown in Figure 5 with resistor values Rp = 0.17 Ω, R_A = 0.036 Ω, and Rs = 0.11 Ω. These values were found using N-C. We also used Φ_{PC}(H-S-0) (2) with Σ_A = 3 S, as shown in Figure 6b, in obtaining J1 and J2 from (15) and (12).

The J2 rise time τ is substituted for L in (21) using (13).

$$\tau = 1.12 \times 10^{14} |\mathrm{Dst}| (\mathrm{Rs} + 2R_A) R_A / (\mathrm{Rs}\Phi_{PC}^2) \qquad (22)$$

Obviously, (22) is inconsistent with (12), as the latter assumes τ is constant. However, we will use (22) in an empirical manner to estimate τ in order to determine J1(t) (15) and J2(t) (12). In (22) we assumed that J2 has reached its maximum value of $\Phi_{PC}/(2R_A)$ = 5.5 MA by the time Dst reached its minimum value (−290 nT). The argument being made that under these conditions (22) is a reasonable approximation to the true rise time. The following value is found for τ.

$$\tau = 5.5\mathrm{h} \qquad \mathrm{L} = 545\mathrm{H} \qquad (23)$$

The J2 rise time τ may be longer than the shielding time, as the shielding time also depends on $\Phi_{PC}/(2R_A)$, as will be shown below. Therefore τ is somewhat longer than the shielding times found by 0.5 hours [*Senior and Blanc*, 1984], ~1 hour [*Fejer*, 1997], or 3–300 min [*Richmond et al.*, 2003]. The total ring current energy at Dst minimum is 6.9×10^{15} J by (21) which is within the usual range of 10^{15}–10^{16} J [*Nagatsuma*, 2002]. Circuit analysis regarding magnetospheric-ionospheric coupling has also been carried out by *Boström* [1964], *Weimer* [1994], and *Block et al.* [1998].

7.5. Shielding

[44] In Figure 8, J1 (15) and J2 (12) are plotted using the resistor values found above and the H-S-O transpolar potential values from Figure 6b. Both J1 and J2 in Figure 8 reach large values later into the storm as observed by *Huang and Burke* [2004]. Now combining J1(t) and J2(t) with the values Eeq1 = 1.0 mV/m and Eeq2 = −2.0 mV/m from Table 1, the time-dependent penetration electric field Eeq(t) (19), as shown in Figure 9, is found. The value Eeq = 1 mV/m corresponds to an upward drift velocity at Jicamarca of 40 m/s [*Fejer*, 1997]. The horizontal line at Eeq = 1.25 mV/m (Figure 9) then corresponds to an upward velocity of ~50 m/s, a value found by Fejer [*Fejer et al.*, 1999] and Whalen [*Whalen*, 2001] as the threshold for the generation of strong spread *F* and the onset of bubbles. Note from Figure 8 that at the beginning of the storm (1643 UT) J1 increases much faster than J2, resulting in an initial positive spike in Eeq(t) (Figure 9). Five bubbles were observed on the DMSP satellites between 1818 and 2037 UT on 06 April 2000. These are indicated by symbols at the bottom of Figure 9 and are explicitly displayed in Figure 10. Looking at Figure 9, it is seen that some of these earlier bubbles could be related to the initial ramping of Eeq. Later into the storm other causes, such the neutral wind dynamo are probably responsible for bubbles. The timing of Eeq dropping below the Fejer-Whalen threshold is very dependent on the equivalent resistor values found for S-RC. For example, if we increase R_A by a factor of two, then Eeq drops below the Fejer-Whalen threshold 2.4 hours later, as seen in Figure 9. The increase in shielding time is due to the effect of R_A on J2 as is easily determined from (12) and (22). Later in the storm, magnetometers on board the DMSP satellites observe Region 2 precipitation currents at low magnetic latitudes ~50°. These currents strongly imply shielding consistent with Figures 8 and 9. Therefore the later bubbles are not produced by penetration electric

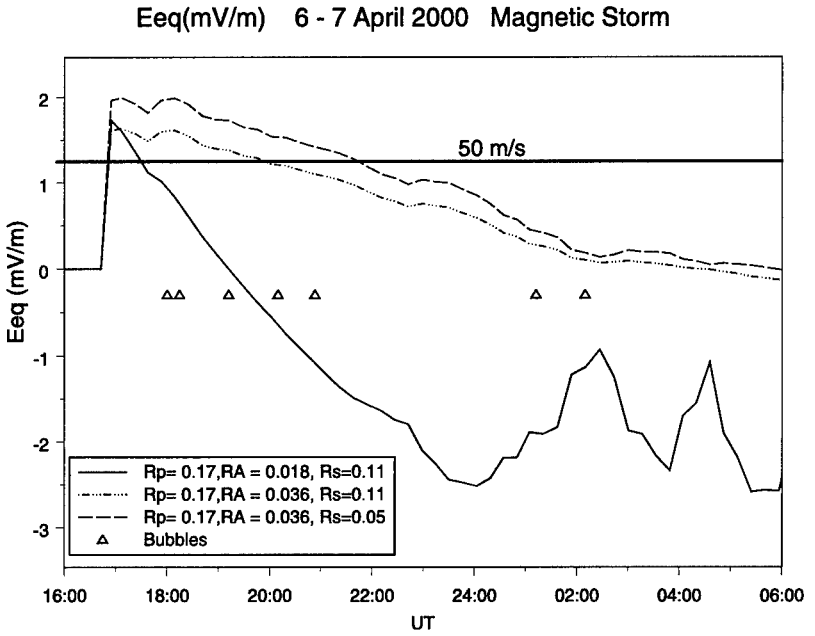

Figure 9. Time-history on 6 April 2000 of Eeq (~1800 MLT) based on the values of J1, J2 as given in Figure 8 and the values of Eeq1 and Eeq2 as given in Table 1 of text for Σ_A = 3 S. The solid line represents our best estimate. An increase in R_A suppresses shielding, as does a decrease in Rs, the low-latitude resistance. All resistance values are in Ohms. In terms of Figure 5 an increase in R_A lengthens the J2 rise-time as well depresses the J2 amplitude (12). A decrease in Rs diverts current through the low-latitudes that otherwise would have contributed to J2. The curves are continued beyond 24:00 to show the relation with the two later bubbles. The solid line represents the Fejer-Whalen [*Fejer et al.*, 1999; *Whalen*, 2001] threshold for the onset of strong spread *F* (i.e., bubbles).

fields. Two bubbles were observed late in the storm on 7 April at 0058 UT and at 0139 UT. (Given the closeness in geographic longitude of the two bubbles, they are probably the same bubble measured by two different satellites.) Mechanisms, such as the ionospheric winds discussed by *Richmond et al.* [2003], may play a key role here [see *Richmond et al.*, 2003, Figure 4]. It should be emphasized that DMSP spacecraft do not detect every bubble due to their altitude (835 km) and orbital period (101 min).

8. Summary

[45] Three models have been combined to form a solar wind-magnetosphere-ionosphere model. Our approach has been to use the strengths of one model to offset deficiencies in the other two. For example, the ionospheric model N-C [*Nopper*, 1978; *Nopper and Carovillano*, 1978, 1979], given J1 and J2, replicates the expected ionospheric features quite well. The J1 current is driven by the solar wind as described by the Hill-Siscoe model [*Hill et al.*, 1976; *Siscoe et al.*, 2002]. The J2 current, according to the S-RC [*Siscoe*, 1982] model, is driven by J1 so that the region-1 and region-2 currents are coupled [*Siscoe*, 1982]. Knowledge of J2 is necessary in order to estimate the penetration electric field. From another point of view, Hill-Siscoe requires knowledge of the polar cap Pedersen conductance to determine the transpolar potential. This is supplied by N-C. In addition, S-RC [*Siscoe*, 1982] uses Hill-Siscoe to define a transpolar potential that drives a simple LR circuit, the resistive element values are defined from N-C. The result is a unified model that gives the time-dependent behavior of the penetration electric field based on the solar wind at L1.

[46] In more detail, we have explored the applicability of Poisson's equation to a two-dimensional conducting ionosphere including dip-angle effects. Following *Nopper and Carovillano* [1978], it was found that such a simple treatment yields two-cell polar cap potentials, electrojets (see Appendix A), as well as giving estimates for the equatorial electric fields in terms of region-1 and -2 currents. The latter was simplified by using the concept of Green's functions. The N-C model provides a systematic procedure for finding the conductance appropriate for the H-S-O model consistent with conductance values at lower latitudes. The resulting values for the H-S-O transpolar potential were found to be in very good agreement with those of the *Weimer* [2005] empirical model (Figure 6a) and DMSP (Figure 6b). The *Siscoe* [1982] ring current model was used to attach a simple magnetospheric circuit to the N-C model. Conductance properties of the N-C model were used to define resistor values in the *Siscoe* [1982] model. In this manner, one can estimate ring current (J2) response to solar wind parameter changes. An equivalent inductance L for the ring current was justified based on the work of *Hines* [1963], who showed that electrical energy was directly stored in ion gyromotion. However, while the Dessler-Parker-Scopke relation allows reasonable J2 rise times to be estimated, there are serious consistency problems regarding L that need to be resolved. Finally, in Figure 9 we estimated the penetration electric field as a function of time. The solid line

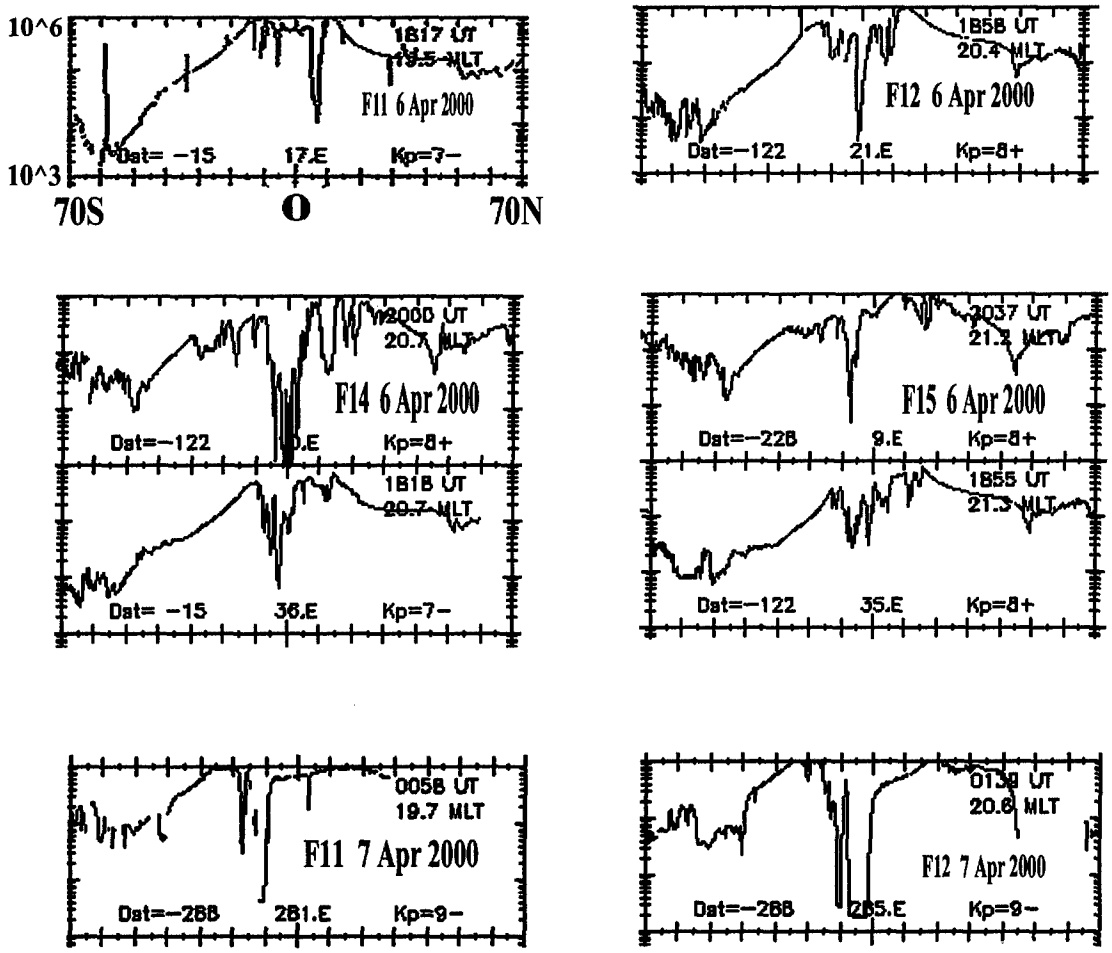

Figure 10. Observations of total ion density at 845 km by DMSP spacecraft on 6–7 April 2000 as a function of the corrected geomagnetic latitude at the subsatellite point. The UT and MLT times in the upper right of each frame and the longitude in the lower, center are values when the spacecraft crossed the magnetic equator. All three spacecraft travel south to north in the evening sector. The abscissa denotes magnetic latitude with zero at the center of each plot and 70°S and 70°N denoting the limits.

represents the case for the resistor values found from the N-C model and indicates that Eeq(t) stayed above the Fejer-Whalen threshold for about an hour after onset. If, however, one doubles the value of R_A in the *Siscoe* [1982] model from 0.018 S to 0.036 S, then Eeq(t) is above the Fejer-Whalen threshold for 3.5 hours as also seen in Figure 9. Therefore even in this simple treatment penetration electric fields are dependent on nonlocal effects, as R_A is one measure of resistance at high latitudes.

9. Discussion

[47] Our coupling of three models, N-C, H-S-O, and S-RC helps to explain the limited duration of electric-field penetration in geophysical terms. The sudden increases in the pressure on the Earth's magnetosphere and the interplanetary electric field almost immediately drove a J1 current, as implied by the H-S-O model. The J1-flow occurs promptly because its source is tied directly to the magnetosheath generator via newly opened magnetic field lines. The agreement between H-S-O and *Wiemer* [2005], as seen in Figure 6a, using N-C under the present assumptions, indicates that the Hill-Siscoe model accurately reflects the dependence of the transpolar potential on the solar wind. Companion J2 currents cannot respond immediately because their source is distributed in the plasma sheet and inner magnetosphere. The pressure gradients needed to drive these currents [*Vasyliunas*, 1970] typically take several hours to grow [*Garner et al.*, 2004], analogous to the response of an inductor. At storm onset the plasma that provides the high-pressure source of J2 current is spread throughout the geomagnetic tail and requires ~3 hours to concentrate in the inner magnetosphere, a timescale that is consistent with the times found above.

[48] Bubbles can form in the postsunset equatorial ionosphere due to the $\mathbf{E} \times \mathbf{B}$ force pushing plasma upwards. *Whalen* [2001] showed that bubbles generally form when the upward ion drift is 50 m/s or greater. If the normal diurnal cycle of equatorial plasma drifts [e.g., *Fejer et al.*, 1999] is augmented by electric-field penetration from high latitudes in sufficient strength to cross the 50 m/s (1.25 mV/m) Fejer-Whalen threshold, then EPBs and accompanying radio-signal scintillations are likely to follow as shown in Figure 9. Note, however, that not all bubbles initiated at

lower altitudes will be observed on DMSP satellites and that other causes such as global winds driven by solar heating or disturbance winds driven by high-latitude heating and ion-drag acceleration, as mentioned by *Richmond et al.* [2003], may also cause bubbles. A zonally propagating gravity wave can also initiate the Rayleigh-Taylor instability in the bottomside F region [*Huang and Kelley*, 1996a, 1996b].

[49] The 6–7 April 2000 storm started at 1643 UT and DMSP spacecraft observed EPBs from ~1817 UT to ~2040 UT. Looking at Figure 9, one sees that Eeq first crossed the Fejer-Whalen threshold at 1655, less than 2 hours before the first bubble was observed at 1818. The second set of bubbles were initiated at 0058 on 7 April, more than 8 hours after Eeq exceeded the Fejer-Whalen threshold, indicating they were probably caused by other mechanisms.

[50] In addition to the increasing strength of J2 currents, both J1 and J2 moved to lower latitudes between 1900 and 2200 UT. More details of this equatorial movement for the 6 April 2000 storm may be seen in Figure 4 of *Huang and Burke* [2004]. Early in the storm (~1707 UT), DMSP observations near the dawn terminator place J1 at ~73°. As previously mentioned, the increase in both model Eeq1 and Eeq2 as J1 and J2 move equatorward compromises the accuracy of Eeq, which is dependent on the difference of the two. Also, we are presently improving the conductivity gradient near the terminator to give us more realistic estimates of Eeq. Both the location of J1 and the strength of J2 need to be modeled as accurately as possible in estimating the point(s) in a storm when the upward plasma drifts reach the threshold for generating EPBs.

[51] We have assumed that the polar conductance remains constant throughout the storm which allowed us to use a linear treatment. However, this approximation may not hold in all cases, particularly when the electron precipitation is very energetic. The solution for the general problem involves an implicit relation for J1 as shown in (24).

$$\Phi_{pc}(N-C) = \frac{J1}{\xi\Sigma_P^p(J1)} = \frac{30P_{sw}^{1/2} + 57.6E_{sw}P_{sw}^{1/3}}{0.0187\xi\Sigma_p^p(J1)P_{sw}^{1/6} + 0.036E_{sw}\xi\Sigma_P^p(J1) + P_{sw}^{1/2}} = \Phi_{pc}(H-S-O) \quad (24)$$

The dependence on J1 enters through its effect on auroral conductance, and therefore $\xi\Sigma_P^p(J1)$ may be numerically found by using N-C to determine $\Phi_{PC}(N\text{-}C)$ for a range of J1.

10. Conclusions

[52] 1. There is agreement between H-S-O and the Weimer model as seen in Figure 6a, since F10.7 ~ 177 for both the present magnetic storm and during the time interval on which the Weimer model [*Weimer*, 2005] is based. The similar values of F10.7 imply the same EUV polar conductance was present in both cases. The agreement also indicates that the N-C model gives reasonable conductance values as input to the H-S-O model.

[53] 2. The N-C and H-S-O models can be made consistent with one another by using N-C to define the equivalent "single-wire" conductance between the potential extremes shown in Figure 2.

[54] 3. The N-C model may be treated as a numeric Green's function provided that the ionospheric conductance and the J1, J2 geometries remain unchanged. By running the two cases J1 = 1 MA, J2 = 0 and J1 = 0, J2 = 1 MA the potential and electric field at any point for arbitrary values of J1, J2 may be obtained. The N-C model can also be made more realistic by adding a conductance gradient at the terminator based on density data. This addition has the effect of shifting the prereversal peak, as shown in Figure 7, from ~2300 MLT to ~1800 MLT.

[55] 4. Using the *Siscoe* [1982] ring current model (S-RC) and knowing the time-dependence of J1 and J2, a time profile for the penetration electric field Eeq(t) can be found as shown in Figure 9. From Figure 9 it is seen that the earlier bubbles are associated with values of Eeq > 1.25 mV/m, consistent with the Fejer-Whalen threshold [*Fejer et al.*, 1999; *Whalen*, 2001], although it should be emphasized that other mechanisms exist, such as ionospheric winds [*Richmond et al.*, 2003], as alternate interpretations.

[56] We have compared and combined the Nopper-Carovillano [N-C], the Hill-Siscoe-Ober,[H-S-O], Siscoe Ring Current (S-RC), and Weimer models in a consistent way (see Figure 6). In this manner, the solar wind has been electrically coupled to the ionosphere.

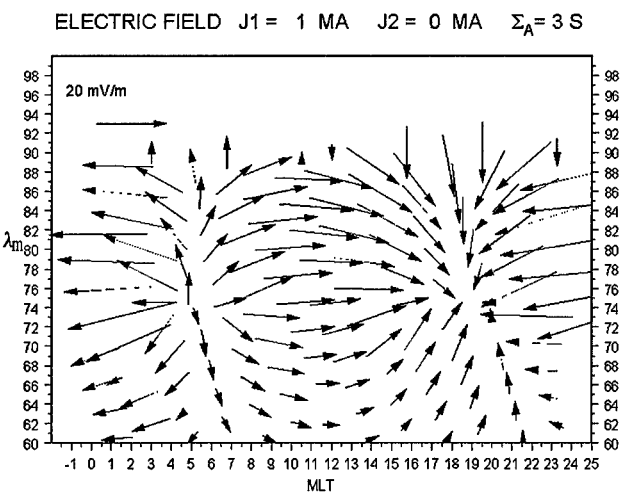

Figure A1. This figure shows the electric field at high latitudes for the ionospheric conductance used in the text (17). Note the positive charge on the dawnside and the negative charge on the duskside.

Appendix A

[57] In this appendix we have two goals. The first goal is to illustrate some of the global features of N-C. The second goal is to demonstrate how ionospheric electric fields and currents can be scaled with the transpolar potential using Table 1 and (2). In this way, estimates may be made, for example, of electrojet intensity as a function of solar wind parameters. Figure A1 shows the electric field vector pattern at high latitudes, as obtained from N-C. Recall for this case that the input to N-C is a uniform region-1 current, forming

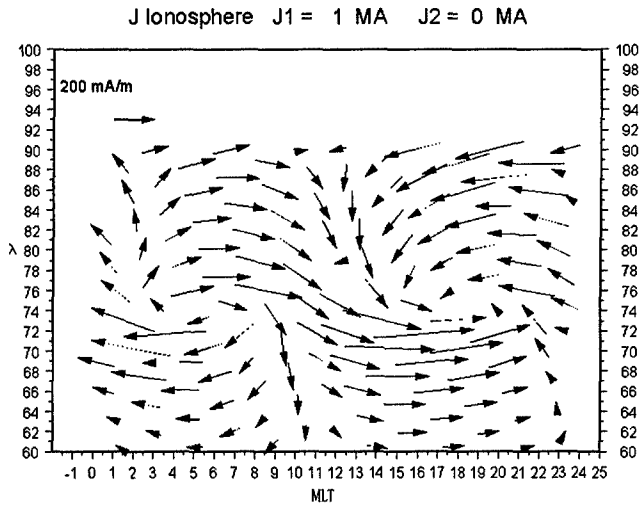

Figure A2. The ionospheric current in amperes per meter at high latitudes. Note that the dominance of the Hall term that leads to electrojet-type properties in the auroral region, a westward electrojet on the dawnside with an eastward electrojet on the duskside. The MLT axis has been expanded to accommodate the arrows at the figure's edges.

a longitudinal-arc of 120° and extending 3° in latitude into the ionosphere on the dawnside, out of the ionosphere on the duskside (see Figures 3 and 4). The N-C model clearly show in Figure A1 that, with the ionospheric conductance given in (17), this is equivalent to placing a positive charge at 0600 MLT and 74° in magnetic latitude and a negative charge of equal magnitude at 1900 MLT, also at 74°. Therefore given the ionospheric conductance profile according to N-C there is a correlation between the geometrical distribution of the region-1 currents and the two-cell polar potential pattern. Returning to Figure A1, the distance between the two charges is ~30° or 3.3×10^6 m. If one now takes the value of 73 kV for Φ_{PC} as given in Table 1 then the average electric field across the polar cap is 22 mV/m, consistent with the arrow lengths shown. If, for example, one wants to know the ionospheric electric field when Φ_{PC} = 180 kV, as determined from (2), one finds from Table 1, J1 = (13.7 × 0.180) = 2.5 MA. This changes the scale factor in Figure A1 from 20 mV/m to 50 mV/m and the average electric field strength to 55 mV/m. In this way, the ionospheric electric fields can be estimated as a function of the solar wind parameters to a zero-order approximation. The term zero-order refers to assuming the polar cap conductance being static throughout the storm and the neglect of other nonlinear processes.

[58] Now let us look at the high-latitude currents. The ionospheric Hall conductance, when impressed by the electric field shown in Figure A1, causes the ionospheric currents to form the pattern shown in Figure A2, a westward electrojet on the dawnside and an eastward electrojet on the duskside. The currents are predominantly Hall currents, forming closed loops over the poles and at lower latitudes. Under the assumption that the electrojets are concentrated between 60° and 72° in magnetic latitude, Figure A2 implies an eastward electrojet of 1.0 MA compared with 0.6 MA for the westward electrojet. On the other hand, if one now numerically integrates the azimuthal current density from 0° to 72° degrees, one finds a total eastward current of 1.4 MA at dusk and a total westward current of 1.1 MA at dawn. In other words, in this model 71% of the eastward current exists above 60° in magnetic latitude in comparison with 55% for the westward current. If we now

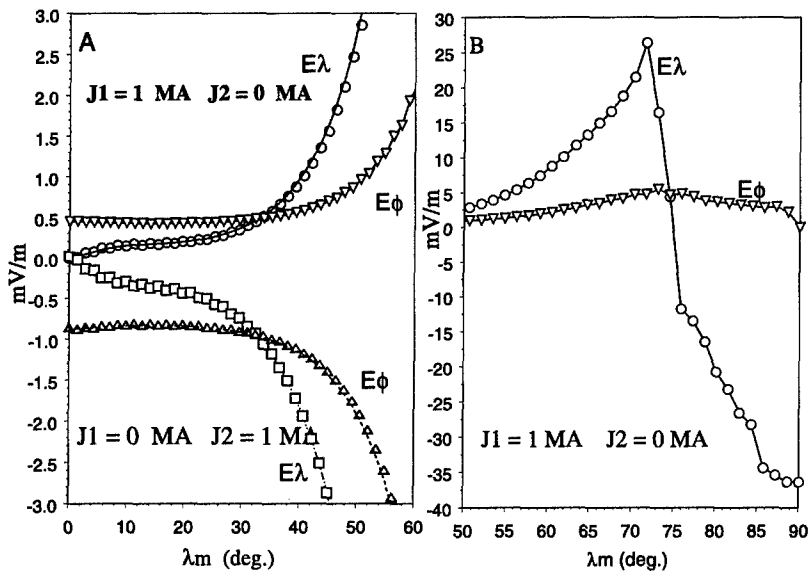

Figure A3. (a) The latitudinal E_λ and azimuthal E_φ components of the electric field for the two cases shown at 1800 MLT. Note that the superposition of the two cases shows the suppression (shielding) of J1 by J2. (b) The same quantities at higher latitudes. The observed divergence in E_λ shows that, for the simple current configuration chosen, the precipitation current manifests itself as a point charge, leading to the potential contours seen in Figures 3 and 4. The negative values of E_λ near the pole arise from the transpolar potential.

multiply these results by 2.5 for the 6–7 April 2000 magnetic storm, as was done above for the electric field, we may estimate the electrojet current values at maximum Φ_{PC}. These values are 2.5 MA and 1.5 MA for the eastward and westward electrojets, respectively.

[59] Figure A3 shows the electric field profile along the 1800 MLT meridian as predicted by N-C. Figure A3a shows two cases with either J1 or J2 = 1 MA with the other being zero. The symbols represent the actual output of the N-C code. The symbol E_λ denotes the poleward electric field component along the magnetic meridian and E_φ the eastward component which, under symmetry, is equal to Eeq. *Nopper and Carovillano* [1978], by requiring symmetry, imposed the boundary condition $E_\lambda = -E_\theta = 0$ at the equator and solved for one hemisphere. We, on the other hand, retain symmetry but treat both hemispheres and do not impose an equatorial boundary condition. Note, however, that for both cases in Figure A3a, $E_\lambda \rightarrow 0$ at the equator ($\lambda m = 0$) consistent with symmetry.

[60] Now one of the main goals of this paper is to estimate Eeq under various high-latitude conditions, where Eeq is the difference between the equatorial E_φ due to J1 and J2. If Eeq is positive, it contributes to stimulating the Rayleigh-Taylor instability for bubble formation. On the other hand, if Eeq is negative it suppresses the instability (overshielding). Figure A1a shows that for J1 = J2 = 1 MA that Eeq = − 0.4 mV/m, which is consistent with overshielding.

[61] Figure A3b shows the high-latitude electric field profiles for J1 = 1 MA, J2 = 0 MA. Recall that for the N-C model in the present instance, the region-1 currents are assumed to be uniform and form a semicircular slab about the dawn and dusk meridians. Under this simplistic condition we see from Figure A3b that there is an equivalent charge density located at the center of the slab. The rather dramatic discontinuity in the slope of E_λ is unrealistic as a result of this simplistic assumption and can easily be removed by adjusting the distribution of J1. Poleward E_λ becomes rapidly negative to reflect the dawn-dusk potential across the polar cap. Note that E_λ dominates over E_φ everywhere but at the ionospheric equator where, as just pointed out, E_λ goes to zero because of symmetry.

[62] In this appendix we have illustrated that N-C despite its conceptual simplicity is a powerful tool in quickly defining the electrical properties of the global ionosphere, as modified by the solar wind. It is argued that N-C gives reasonable zero-order estimates for the ionospheric electric field and may be modified in a systematic way to explain detailed observations.

[63] **Acknowledgments.** We would like to express our appreciation to William J. Burke, Frederick J. Rich, James A. Whalen, David L. Cooke, and Edmond M. Dewan for their assistance and comments, as well as Odile de la Beaujardiere for her advice and comments. George Siscoe of Boston University and Carl-Gunne Fälthammar of the Royal Institute of Technology, Stockholm, Sweden were also very helpful in their comments. We would also like to thank Daniel Weimer from ATK Mission Research of Nashua, New Hampshire for his latest potential code and Neil Grossbard for his programming help. This work was done under AFOSR Task 2311SDA3. Dst values were obtained from the World Data Center, Kyoto (http://swdcwww.kugi.kyotou.ac.jp/index.html). Interplanetary environment data were obtained from the ACE Web site (http://www.srl.caltech.edu/ACE/).

[64] Arthur Richmond thanks Richard A. Wolf and another reviewer for their assistance in evaluating this paper.

References

Basu, S., Su Basu, K. M. Groves, H.-C. Yeh, S.-Y. Su, F. J. Rich, P. J. Sultan, and M. J. Keskinen (2001), Response of the equatorial ionosphere in the South Atlantic region to the great magnetic storm of July 15, 2000, *Geophys. Res. Lett.*, *28*(18), 3577–3580.

Block, L. P., C.-G. Fälthammar, P. L. Rothwell, and M. B. Silevitch (1998), Advantages of electric circuit models for treating the substorm breakup problem, *J. Geophys. Res.*, *103*(A4), 6913–6916.

Boström, R. (1964), A model of the auroral electrojets, *J. Geophys. Res.*, *69*, 4983–4999.

Boyle, C. P., P. H. Reiff, and M. R. Hairston (1997), Empirical polar cap potentials, *J. Geophys. Res.*, *102*(A1), 111–126.

Briggs, W. L., V. E. Henson, and S. F. McCormick (2000), *A Multigrid Tutorial*, 2nd ed. Soc. for Indust. and Appl. Math., Philadelphia, Pa.

Crooker, N. U., and G. L. Siscoe (1983), Ring coupling model: Implications for substorm onset, *Geophys. Res. Lett.*, *10*, 761–764.

Dessler, A. J., and E. N. Parker (1959), Hydromagnetic theory of geomagnetic storms, *J. Geophys. Res.*, *64*, 2239–2252.

Fejer, B. G. (1997), The electrodynamics of the low-latitude ionosphere: Recent results and future challenges, *J. Atmos. Sol. Terr. Phys.*, *59*(13), 1465–1482.

Fejer, B. G. (2003), Solar wind-magnetosphere effects in the middle and low latitude ionosphere, in *Proceedings of the International Symposium on Auroral Phenomena and Solar-Terrestrial Relations*, Space Res. Inst., Russian Acad. of Sci., Moscow.

Fejer, B. G., and L. Scherliess (1997), Empirical models of storm time equatorial zonal electric fields, *J. Geophys. Res.*, *102*(A11), 24,047–24,056.

Fejer, B. J., D. T. Farley, R. F. Woodman, and C. Calderon (1979), Dependence of equatorial *F* region vertical drifts on season and solar cycle, *J. Geophys. Res.*, *84*(A10), 5792–5802.

Fejer, B. G., R. W. Spiro, R. A. Wolf, and J. C. Foster (1990), Latitudinal variation of perturbation electric fields during magnetically disturbed periods: 1986 SUNDIAL observations and model results, *Ann. Geophys.*, *94*(8), 441–445.

Fejer, B. G., E. R. dePaula, S. A. Gonzales, and R. F. Woodman (1991), Average vertical and zonal F region plasma drifts over Jicamarca, *J. Geophys. Res.*, *96*(A10), 13,901–13,906.

Fejer, B. G., W. B. Hanson, and R. A. Heelis (1993), Satellite observations of low-latitude ionospheric plasma depletions, in *Proceedings of the COSPAR Colloquium on Low-Latitude Ionospheric Physics*, edited by F.-S. Kuo, pp. 51–56, Pergamon, New York.

Fejer, B. G., L. Scherliess, and E. R. de Paula (1999), Effects of the vertical plasma drift velocity on the generation and evolution of equatorial spread *F*, *J. Geophys. Res.*, *104*(A9), 19,859–19,869.

Garner, T. W., R. A. Wolf, R. W. Spiro, W. J. Burke, B. G. Fejer, S. Sazykin, J. L. Roederer, and M. R. Hairston (2004), Magnetospheric electric fields and plasma sheet injection to low-L shells during the 4–5 June 1991 magnetic storm, *J. Geophys. Res.*, *109*, A02214, doi:10.1029/2003JA010208.

Gonzales, C. A., M. C. Kelly, B. G. Fejer, J. F. Vickery, and R. F. Woodman (1979), Equatorial electric fields during magnetically disturbed conditions: 2. Implications of simultaneous auroral and equatorial measurements, *J. Geophys. Res.*, *84*, 5803–5812.

Gonzales, C. A., M. C. Kelley, R. A. Behnke, J. F. Vickrey, R. Wand, and J. Holt (1983), On the latitude variations of the ionospheric electric field during magnetic disturbances, *J. Geophys. Res.*, *88*(A11), 9135–9144.

Greenspan, M. E., C. E. Rasmussen, W. J. Burke, and M. A. Abdu (1991), Equatorial density depletions observed at 840 km during the great magnetic storm of March 1989, *J. Geophys. Res.*, *96*(A8), 13,931–13,942.

Heppner, J. P., and N. C. Maynard (1987), Empirical high-latitude electric field models, *J. Geophys. Res.*, *92*(A5), 4467–4489.

Hill, T. W., A. J. Dessler, and R. A. Wolf (1976), Mercury and Mars: The role of ionospheric conductance in the acceleration of magnetospheric particles, *Geophys. Res. Lett.*, *3*(8), 429–433.

Hines, C. O. (1963), The energization of plasma in the magnetosphere: Hydromagnetic and particle-drift approaches, *Planet. Space Sci.*, *10*, 239–246.

Huang, C.-S., and M. C. Kelley (1996a), Nonlinear evolution of spread F: 1. On the role of plasma instabilities and spatial resonance associated with gravity waves, *J. Geophys. Res.*, *101*(A1), 283–292.

Huang, C.-S., and M. C. Kelley (1996b), Nonlinear evolution of spread F: 2.Gravity wave seeding of Rayleigh-Taylor instability, *J. Geophys. Res.*, *101*(A1), 293–302.

Huang, C. Y., and W. J. Burke (2004), Transient sheet of field-aligned current observed by DMSP during the main phase of a magnetic super storm, *J. Geophys. Res.*, *109*, A06303, doi:10.1029/2003JA010067.

Huang, C. Y., W. J. Burke, J. S. Machuzak, L. C. Gentile, and P. J. Sultan (2001), DMSP observations of equatorial plasma bubbles in the topside ionosphere near solar maximum, *J. Geophys. Res.*, *106*(A5), 8131–8142.

Huang, C. Y., W. J. Burke, J. S. Machuzak, L. C. Gentile, and P. J. Sultan (2002), Equatorial plasma bubbles observed by DMSP satellites during a full solar cycle: Toward a global climatology, *J. Geophys. Res.*, *107*(A12), 1434, doi:10.1029/2002JA009452.

Iijima, T., and T. A. Potemra (1976), The amplitude distribution of field-aligned currents at northern high latitudes observed by Triad, *J. Geophys. Res.*, *81*(13), 4611–4619.

Kelley, M. C., J. J. Makela, J. L. Chau, and M. J. Nicolls (2003), Penetration of the solar wind electric into the magnetosphere/ionosphere system, *Geophys. Res. Lett.*, *30*(4), 1158, doi:10.1029/2002GL016321.

Kivelson, M. G., and C. T. Russell (Eds.) (1997), *Introduction to Space Physics*, Cambridge Univ. Press, New York.

Nagatsuma, T. (2002), 3–5 Geomagnetic storms, *J. Comm. Res. Lab.*, *49*(3), 139–154.

Nopper, R. W., Jr. (1978), Ionospheric electric fields and currents of magnetospheric origin, Ph.D. thesis, Boston Coll., Chestnut Hill, Mass.

Nopper, R. W., Jr., and R. L. Carovillano (1978), Polar-equatorial coupling during magnetically active periods, *Geophys. Res. Lett.*, *5*(8), 699–702.

Nopper, R. W., Jr., and R. L. Carovillano (1979), On the orientation of the polar cap electric field, *J. Geophys. Res.*, *84*(A11), 6489–6492.

Ober, D. M., N. C. Maynard, and W. J. Burke (2003), Testing the Hill model of transpolar potential saturation, *J. Geophys. Res.*, *108*(A12), 1467, doi:10.1029/2003JA010154.

Press, W., S. A. Teukolsky, W. T. Vetterling, and B. P. Flannery (1992), *Numerical Recipes: The Art of Scientific Computing*, 2nd ed., Cambridge Univ. Press, New York.

Rich, F. J., and M. Hairston (1994), Large-scale convection patterns observed by DMSP, *J. Geophys. Res.*, *99*(A3), 3827–3844.

Richmond, A. D., C. Peymirat, and R. G. Roble (2003), Long-lasting disturbances in the equatorial ionospheric electric field simulated with a coupled magnetosphere-ionosphere-thermosphere model, *J. Geophys. Res.*, *108*(A3), 1118, doi:10.1029/2002JA009758.

Robinson, R. M., and R. R. Vondrak (1984), Measurements of E region ionization and conductivity produced by solar illumination at high latitudes, *J. Geophys. Res.*, *89*(A6), 3951–3956.

Robinson, R. M., R. R. Vondrak, K. Miller, T. Dabbs, and D. A. Hardy (1987), On calculating the ionospheric conductivities from the flux and energy of precipitating electrons, *J. Geophys. Res.*, *92*(A3), 2565–2569.

Scherliess, L., and B. G. Fejer (1997), Storm time dependence of equatorial disturbance dynamo electric fields, *J. Geophys. Res.*, *102*(A11), 24,037–24,046.

Scopke, N. (1966), A general relation between the energy of trapped particles and the disturbance field over the Earth, *J. Geophys. Res.*, *71*, 3125–3130.

Senior, C., and M. Blanc (1984), On the control of magnetospheric convection by the spatial distribution of ionospheric conductivities, *J. Geophys. Res.*, *89*(A1), 261–284.

Siscoe, G. L. (1982), Energy coupling between Regions 1 and 2 Birkland current systems, *J. Geophys. Res.*, *87*(A7), 5124–5130.

Siscoe, G. L., and T. S. Huang (1985), Polar cap inflation and deflation, *J. Geophys. Res.*, *90*(A1), 543–547.

Siscoe, G., and N. Maynard (1991), Distributed two-dimensional Region 1 and Region 2 currents: Model results and data comparisons, *J. Geophys. Res.*, *96*(A12), 21,071–21,086.

Siscoe, G. L., G. M Erickson, B. U. O. Sonnerup, N. C. Maynard, J. A. Shoendorf, K. D. Siebert, D. R. Weimer, W. W. White, and G. R. Wilson (2002), Hill model of transpolar potential saturation: Comparison with MHD simulations, *J. Geophys. Res.*, *107*(A6), 1075, doi:10.1029/2001JA000109.

Siscoe, G., J. Raeder, and A. J. Ridley (2004), Transpolar potential saturation models compared, *J. Geophys. Res.*, *109*, A09203, doi:10.1029/2003JA010318.

Smiddy, M., W. J. Burke, M. C. Kelley, N. A. Saflekos, M. S. Gussenhoven, D. A. Hardy, and F. J. Rich (1980), Effects of high-latitude conductivity on observed convection electric fields and Birkeland currents, *J. Geophys. Res.*, *85*(12), 6811–6818.

Sonnerup, B. U. O. (1974), Magnetopause reconnection rate, *J. Geophys. Res.*, *79*(10), 1546–1549.

Spiro, R. W., R. A. Wolf, and B. G. Fejer (1988), Penetration of high-latitude-electric-field effects to low latitudes during SUNDIAL 1984, *Ann. Geophys.*, *6*(1), 39–50.

Trottenberg, U., C. Oosterlee, and A. Schüller (2001), *Multigrid*, Elsevier, New York.

Vasyliunas, V. M. (1970), Mathematical models of magnetospheric convection and its coupling to the ionosphere, in *Particles and Fields in the Magnetosphere*, edited by B. M. McCormac, p. 60, Springer, New York.

Weimer, D. R. (1994), Substorm time constants, *J. Geophys. Res.*, *99*(A6), 11,005–11,015.

Weimer, D. R. (1995), Models of high-latitude electric potentials derived with a least error fit of spherical harmonic coefficients, *J. Geophys. Res.*, *100*(A10), 19,595–19,607.

Weimer, D. R. (2001), An improved model of ionospheric electric potentials including substorm perturbations and applications to the Geospace Environment Modeling November 24, 1996 event, *J. Geophys. Res.*, *106*(A1), 407–416.

Weimer, D. R. (2005), Improved electrodynamic models and application to calculating Joule heating rates, *J. Geophys. Res.*, *110*, A05306, doi:10.1029/2004JA010884.

Whalen, J. A. (2001), The equatorial anomaly: Its quantitative relation to equatorial bubbles, bottomside spread F, and E × B drift velocity during a month at solar maximum, *J. Geophys. Res.*, *106*(A12), 29,125–29,132.

Wolf, R. A. (1970), Effects of ionospheric conductivity on convective flow of plasma in the magnetosphere, *J. Geophys. Res.*, *75*(25), 4677–4698.

Woodman, R. F. (1970), Vertical drift velocities and east-west electric fields at the magnetic equator, *J. Geophys. Res.*, *75*(31), 6249–6259.

Zmuda, A. J., and J. C. Armstrong (1974a), The diurnal variation of the region with vector magnetic field changes associated with field-aligned currents, *J. Geophys. Res.*, *79*(16), 2501–2502.

Zmuda, A. J., and J. C. Armstrong (1974b), The diurnal flow pattern of field-aligned currents, *J. Geophys. Res.*, *79*(31), 4611–4619.

J. R. Jasperse and P. L. Rothwell, Space Vehicles Directorate, Air Force Research Laboratory, Hanscom Air Force Base, Bedford, MA 01731, USA. (john.jasperse@hanscom.af.mil; paul.rothwell@hanscom.af.mil)